ACS APPLIED MATERIALS & INTERFACES

Research Article

Cite This: ACS Appl. Mater. Interfaces 2019, 11, 37139−37146

www.acsami.org

Fabrication of Tough Hydrogel Composites from Photoresponsive Polymers to Show Double-Network Effect

Zhen Tao,[†] Hailong Fan,[§] Junchao Huang,[‡] Taolin Sun,[‡,∥,⊥] Takayuki Kurokawa,[‡,∥] and Jian Ping Gong*[,‡,§,∥]

[†]Graduate School of Life Science and [‡]Faculty of Advanced Life Science, Hokkaido University, N21W11, Kita-ku, Sapporo 001-0021, Japan

[§]Institute for Chemical Reaction Design and Discovery (WPI-ICReDD) and [∥]Global Station for Soft Matter, GI-CoRE, Hokkaido University, N21W10, Kita-ku, Sapporo 001-0021, Japan

[⊥]South China Advanced Institute for Soft Matter Science and Technology, South China University of Technology, 381st Wushan Road, Tianhe District, Guangzhou 510640, China

Supporting Information

ABSTRACT: Inspired by the toughening mechanism of double-network (DN) gels, tough hydrogel composites with a sandwich structure were fabricated from photoresponsive polymers. By copolymerization of hydrophilic monomers, 2-ureidoethyl methacrylate (UM), and photoresponsive hydrophobic monomers, (2-nitrobenzyloxycarbonylaminoethyl methacrylate (NBOC)) at high concentrations, physical hydrogels that are soft and highly stretchable are formed due to the hydrophobic associations of NBOC, serving as dynamic crosslinkers. By UV irradiation, the physical crosslinking switches into chemical crosslinking, and the soft physical hydrogels transform into rigid and less stretchable chemical hydrogels. By UV curing the surface layers of the physical hydrogels, we prepared hydrogel composites having a sandwiched structure with two rigid outer layers and a soft inner layer. The molecular-level continuous interfaces and matched swelling ratios between the layers ensure the macroscale hydrogel composites' high strength and toughness with a DN gel effect. The outer layers fracture preferentially at deformation, playing a role like the first network of a DN gel, while the inner layer maintains the integrity, playing a role resembling the second network. The evolution of the fracture morphology of the rigid layers gives useful insight into the internal fracture process of DN gels.

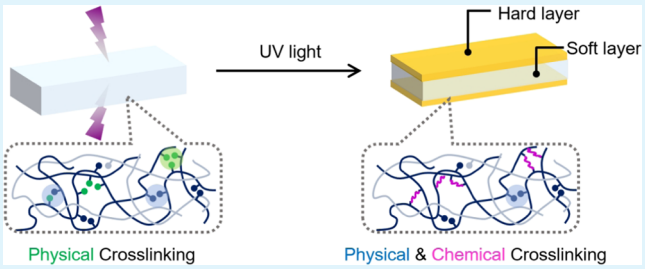

KEYWORDS: *photoresponsive, tough hydrogels, hydrogel composites, DN hydrogel, toughening mechanism, sandwich structure*

INTRODUCTION

Since the first report of double-network (DN) hydrogel in 2003,[1] which has high strength and toughness but containing 90% water, the tough soft matters (hydrogels and elastomers) have achieved great development based on the DN concept. For instance, the failure stress for DN-type hydrogels can easily reach tens of MPa nowadays.[2] Meanwhile, the toughening mechanism of DN hydrogels has been investigated for many years.[3] It is clarified that the special interpenetrated network structure in DN gels plays a key role in the toughening mechanism. Specifically, a DN gel has two polymer networks of very different structures and properties: a densely crosslinked, fully stretched network from a polyelectrolyte (the first network, as a rigid skeleton) and a sparsely crosslinked, modestly stretched network from a neutral polymer (the second network, as a ductile substance). During deformation, the first network (rigid skeleton) ruptures into fragmentation first, while the second network (ductile substance) maintains the integrity and gives a large extension of the materials after the fracture of the first network. Thus, the covalent bonds of the first network act as sacrificial bonds and the second network chains act as hidden length. Such a fracture process, referred to as internal fracture, macroscopically appears as mechanical yielding,[4] which is accompanied by a necking phenomenon. The latter is regarded as the coexistence of the damaged and undamaged zones.[5] Based on this phenomenon, various models and hypothesis have been proposed to explain the molecular mechanism of DN gels.[2,3] However, the direct observation of the internal fracture morphology of DN gels, at a micrometer scale, is still unachievable.

Inspired by the strategy of DN gels, tough composites from two mechanically different components were developed by applying a similar toughening mechanism of DN gels in macroscale.[6−8] For example, Feng et al. fabricated a soft composite consisting of a macroscale nylon fabric mesh as a rigid component and VHB tape layers as a soft component,

Received: August 2, 2019
Accepted: September 17, 2019
Published: September 17, 2019

DOI: 10.1021/acsami.9b13746
ACS Appl. Mater. Interfaces 2019, 11, 37139−37146

Scheme 1. (a) Synthesis Routine of P(UM-*co*-NBOC) Hydrogels and the P(UM-*co*-AMA) Hydrogels; (b) Chemical Structure of Starting Monomers; (c) Phototriggered Self-Immolative Reaction; (d) Subsequent Chemical Cosslinking Following the Self-Immolative Reaction; (e) Schematic Illustration of Fabrication of Hydrogel Composites with the Sandwich Structure

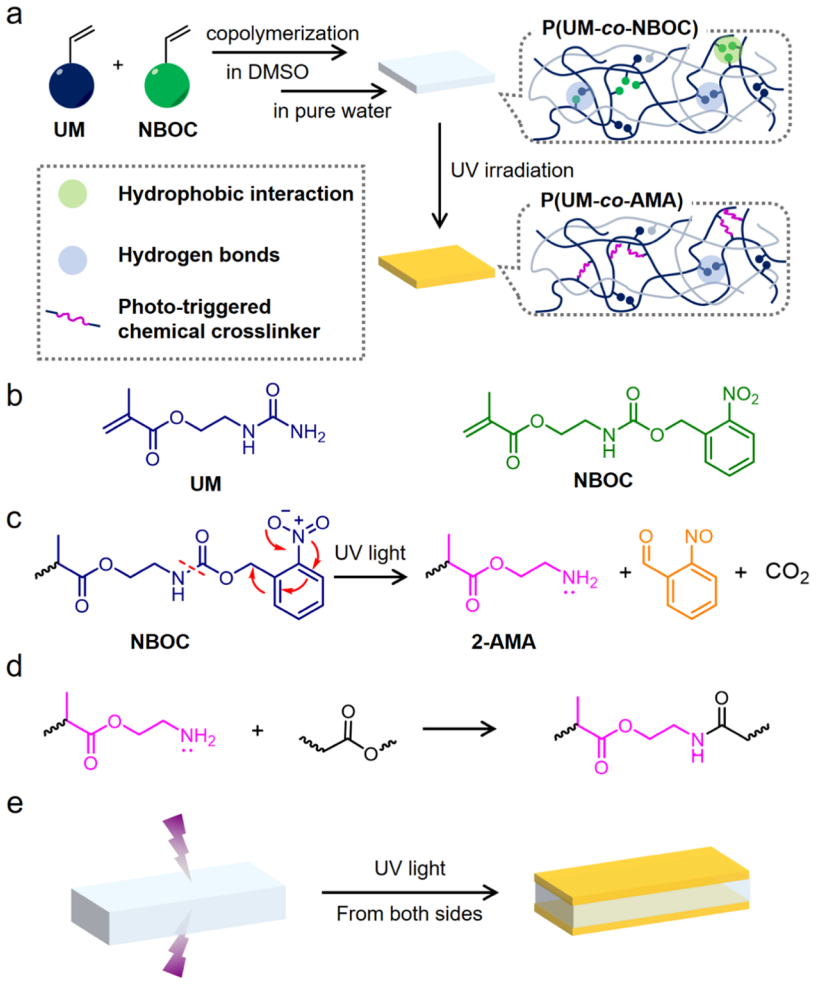

and found that the deformation process is similar to that of DN gel: the fabric mesh fragmented into small islands surrounded by the highly stretched tapes.[6] Recently, our group also developed composites by combining low-melting-point alloy with a macroscale honeycomb structure and hydrogels,[7] and observed the multistep damage process of the rigid honeycomb alloy, similar to that of the DN gels. These results indicate that the macroscale composites possess the same mechanical feature and toughening mechanism as the DN gels that are nanoscale composites.

In this work, we intend to develop macroscale hydrogel composites showing the double-network effect. There are several challenges. First, the soft matrix must be highly stretchable and possess a higher strength than the rigid skeleton.[6−8] Otherwise, the fracture of the rigid skeleton causes catastrophic failure of the material without showing a multistep fracture of the rigid skeleton. Therefore, we need to develop energy-dissipating tough hydrogels as soft matrixes, by the introduction of reversible crosslinkers.[9−11] The swelling mismatching and interface between the soft and rigid phases present another challenge for the hydrogel composites.[7,12] The interface between heterogeneous phases in composite material plays an essential role in force transmission and dissipation of energy, resulting in effective reinforcement on the mechanical properties.[13] In general, hydrogel composites are formed by polymerization in the presence of hard phases such as particles, fibers, and layer elements as the reinforcing components,[12,14,15] where the rigid surface and hydrogels are usually integrated by chemical anchoring or physical adhesion.[16−22] The swelling mismatch between soft and rigid phases lead to surface wrinkle, bulk deformation, or even fracture of materials.[23−25]

To overcome the difficulties mentioned above, we present a facile strategy to prepare hydrogel composites with the continuous interface by designing and developing photo-responsive polymers (Scheme 1). We synthesized copolymers from hydrophilic 2-ureidoethyl methacrylate (UM) and hydrophobic photoresponsive (2-nitrobenzyloxycarbonylaminoethyl methacrylate (NBOC)) (Scheme 1). The NBOC residues in the P(UM-*co*-NBOC) copolymers play two roles. One is working as physical crosslinkers based on their hydrophobic association, which can dissipate a large amount of energy during deformation so as to toughen the hydrogels and the other is providing photoresponsiveness to switch the physical crosslinking to chemical crosslinking.[26] Upon UV irradiation, the 2-nitrobenzyl functional group of NBOC exhibits photo-labile characteristics, with the release of 2-nitrobenzaldehyde and CO_2. In this process, the hydrophobic NBOC groups transform into hydrophilic 2-aminoethyl methacrylate (AMA), leading to disassembly of physical crosslinkers by hydrophobic interaction. However, the

DOI: 10.1021/acsami.9b13746
ACS Appl. Mater. Interfaces 2019, 11, 37139−37146

resulting amino groups of AMA would further attack close-by ester bonds of UM or NBOC to form new chemical crosslinkers. As a result, after UV irradiation, the physical P(UM-*co*-NBOC) gels transform into chemical P(UM-*co*-AMA) gels without a significant change in the swelling ratio. Such photoswitching of physical gels to chemical gels brings about a dramatic change in the mechanical behavior of the hydrogels from soft and highly stretchable to rigid and less stretchable. By controlling UV irradiation, the NBOC-based hydrogels can be easily reconstructed into various composites. As an example, we fabricated sandwich hydrogels composed of rigid chemical hydrogels in the outer layers and soft physical hydrogels in the middle layer. The composite hydrogels, having a strong interface and negligible swelling mismatching, are mechanically tough showing features similar to the DN hydrogels,[27,28] where the hard layers, P(UM-*co*-AMA), play a role of the first network, imparting high modulus and rupturing to dissipate energy, and the soft layer, P(UM-*co*-NBOC), plays a role of the second network, maintaining the global integrity. The macroscale fracture process of this composite gives insight into understanding the microscale fracture process of DN gels.

EXPERIMENTAL SECTION

Materials. 2-Nitrobenzyloxycarbonylaminoethyl methacrylate (NBOC) was synthesized according to the literature.[26] 2-Ureidoethyl methacrylate (UM) was provided by Osaka chemicals Co., Ltd. 2,2′-Azobisisobutyronitrile (AIBN, 98%) was purchased from Sigma-Aldrich. Dimethyl sulfoxide (DMSO) was purchased from Wako Pure Chemical Industries, Ltd. All chemicals were used as received.

Synthesis of Hydrogels. The monomers with different monomer molar ratios were first dissolved in their co-solvent DMSO. For the P(UM-*co*-NBOC) system, the pre-gel solution contains 1.5 M monomers of UM and NBOC mixture with a proscribed NBOC molar fraction (f_{NBOC}), and 0.003 M AIBN (initiator). The total monomer concentration was chosen to be high enough so that the polymers formed are well above their entanglement concentration.

The pre-gel solution was then poured into in a reaction cell consisting of a pair of glass plates with a spacer of prescribed thickness, and the reaction cell was heated at 70 °C for 8 h for thermal polymerization. After polymerization, the as-prepared gel was immersed in a large amount of water for 1 week to reach equilibrium. The hydrogels were coded as P(UM-*co*-NBOC)-f_{NBOC}.

Characterization of Hydrogels. *Swelling Ratio Measurements.* The as-prepared gel was cut into samples with prescribed sizes and then immersed in a large amount of pure water until reaching equilibrium. The swelling volume ratio Q_v was defined as the ratio of the sample volume at swelling equilibrium V to that in the as-prepared state V_0, $Q_v = V/V_0$.

Water Content Measurement. The water content (C_w, wt %) of hydrogel samples were measured with a moisture balance (MOC-120H, SHIMADZU Co., Japan) based on the equation, $C_w = (m_w/m_g) \times 100\%$, where m_w (g) is the weight of water in the hydrogel network, and m_g (g) is the weight of the whole hydrogel sample.

Mechanical Test. Uniaxial tensile tests were performed on hydrogels using a tensile−compressive tester (Instron 5965 type universal testing system) in air. The cyclic tensile stress−strain measurements were performed using a tensile-compressive tester (Tensilon RTC-1310A, Orientec Co.) in a water bath to prevent water from evaporating from the samples. The dissipated energy (U_{hys}) at a prescribed deformation was calculated from the hysteresis area, and the fraction of dissipated energy in relation to total energy applied to the sample (U_{hys}/W) was calculated from the ratio of the hysteresis area U_{hys} to the overall area W below the loading curve. W is the work of extension for a prescribed deformation. The hysteresis recovery ratio was calculated from the ratio of the hysteresis area in the prescribed cycle U_{hys} to the hysteresis area U_{hys} of the first cycle in the cyclic loading−unloading test.

All tests were carried out on dumbbell-shaped samples with the standard JIS-K6251-7 size (12 mm (L) × 2 mm (d)). The sample thickness was 0.3−3 mm (w) depending on the thickness of the reaction cell spacer and the sample formulation. All tests were performed at a deformation velocity of 100 mm/min, corresponding to a stretch rate of 0.14 s^{-1}.

UV Irradiation for Chemical Crosslinking. UV irradiation on samples was conducted on a UV-light-emitting diode irradiation panel (UAW365-31110-1212F, Sentech Co.). The intensity of UV irradiation was 1.78 × 10^4 mJ/cm^2. The hydrogel samples were immersed in a cell of water to prevent water evaporation from the samples during irradiation. The cell consists of a pair of glass plates with a spacer.

Formation of Chemical Crosslinking via ATR/FT-IR. To confirm the formation of chemical crosslinking triggered by UV irradiation, attenuated total reflection Fourier-transform infrared spectroscopy (ATR/FT-IR) on an FT-IR 6600 spectrometer (JASCO, Japan) with a diamond prism was performed.

Optical Microscope Observation. To observe the microcrack formation under stretching, the hydrogel samples after UV irradiation were fixed under various elongation ratios by a tailor-made stretching device,[29] and were observed under an optical microscope (Nikon, Eclipse, LV100POL).

RESULTS AND DISCUSSION

Hydrogel before UV Irradiation as a Soft Component (Second Network). The copolymers P(UM-*co*-NBOC) formed were entangled and physically crosslinked by hydrogen bonding between UM residues to form physical organogel in DMSO. The organogel was then immersed in water to remove the DMSO and unreacted monomers. During the solution replacement process, the NBOC residues aggregated into the hydrophobic domain working as physical crosslinks. As a result, the hydrogels at equilibrium state shrank, compared with the original organogel (Figure 1). This phenomenon becomes more obvious with elevating the NBOC fraction (f_{NBOC}).

The formation of physical crosslinkers by hydrophobic interactions between NBOC residues significantly enhances

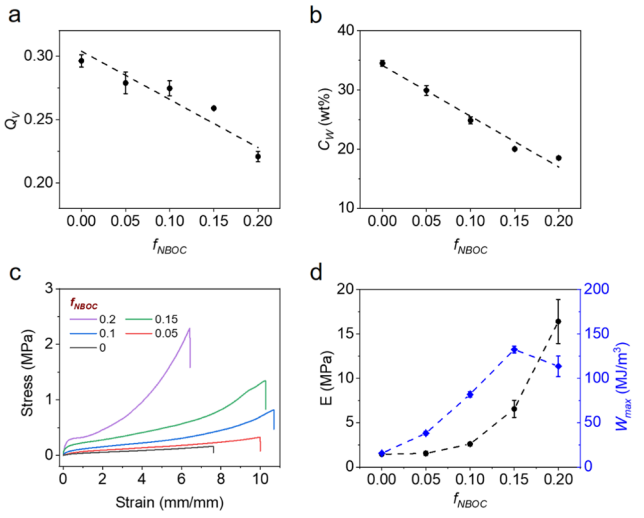

Figure 1. Physical properties and tensile behaviors for P(UM-*co*-NBOC) hydrogels. (a) Volume ratio of samples in water in relation to that in DMSO, Q_V, (b) water content, (c) tensile stress−strain curves, and (d) Young's modulus (E) and work of extension to fracture (W_{max}) of samples with different NBOC molar fraction f_{NBOC}. Each data was the average of 3−5 specimens of the same composition samples. Error bars represent standard deviation.

DOI: 10.1021/acsami.9b13746
ACS Appl. Mater. Interfaces 2019, 11, 37139−37146

the mechanical properties of hydrogels (Figure 1c,d). With the increase of f_{NBOC}, Young's modulus and fracture stress of hydrogels increased, whereas the fracture strain increased with the addition of a small amount of NBOC, but then decreased when f_{NBOC} reached 0.2 (Figure 1c). The toughness of the hydrogels, reflected by work of extension to sample failure (W_{max}), enhanced gradually with the increase in f_{NBOC}. For the P(UM-*co*-NBOC)-0.2 sample, the abrupt decrease in extensibility brought about a slight decrease in toughness. The increase of the NBOC residues results in increasing of the amount of physical crosslinkers and decreasing in the volume of hydrogels, which accounts for the dramatic increase in Young's modulus and strength and decrease of extensibility.

To further investigate the role of the hydrophobic interaction in hydrogel toughness, loading−unloading tests were conducted to evaluate the hysteresis or energy dissipation of hydrogels (Figure 2a,b). Distinct yielding and hysteresis

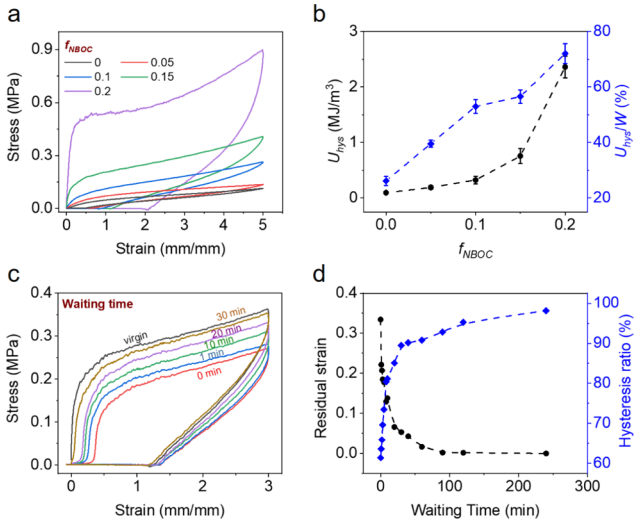

Figure 2. Hysteresis behavior and self-recovery of P(UM-*co*-NBOC) hydrogels. (a) Loading−unloading curves, (b) dissipated energy (U_{hys}) calculated from the hysteresis area and energy dissipation coefficient (U_{hys}/W) of hydrogels with different f_{NBOC} for a strain of 5. Each data was the average of 3−5 specimens of the same composition samples. Error bars represent standard deviation. (c) Cyclic loading−unloading curves and (d) residual strain and the hysteresis recovery ratio between the second and first loading cycles for different waiting times of sample with f_{NBOC} = 0.15.

were observed in the loading−unloading cycle of hydrogels. The amount of dissipated energy U_{hys} and the fraction of energy dissipation in relation to the total input energy, U_{hys}/W, increased with f_{NBOC}. For instance, the U_{hys} of the sample with f_{NBOC} = 0.2 was 2.36 MJ/m^3, and the corresponding fraction of energy dissipation is as high as 72% for strain 5, which is 25 times (U_{hys}) of the pure PUM hydrogels (f_{NBOC} = 0) (Figure 2a). This indicates that most of the energy used for deformation is dissipated by breaking a large amount of hydrophobic interactions.

The broken physical crosslinkers, through which energy is dissipated during deformation of hydrogel samples, reform subsequently. Thus, the dynamic and reversible feature of physical crosslinkers endowed the hydrogel with good self-recovery behavior and fatigue resistance. Cyclic loading−unloading tensile tests were performed to investigate the self-recovery ability of P(UM-*co*-NBOC) hydrogels (Figure 2c,d). The P(UM-*co*-NBOC)-0.15 hydrogel was chosen as a representative because of its relatively large U_{hys} and the fraction of energy dissipation of the first loading−unloading cycle. After 240 min waiting of the first loading−unloading cycle, the hydrogel could recover to 100% of the virgin state (Figure 2d). The sample showed obvious residual strain right after unloading (Figure 2d), while the residual strain completely disappeared after a relatively short waiting time (20 min), and the sample recovered to the virgin state fully. The waiting time dependences of residual strain and the hysteresis ratio between the second cycle to the first cycle indicate that the self-recovery consists of two stages, the initial fast stage and later slow stage, which is similar to other tough hydrogels with physical sacrificial bonds, including polyampholyte hydrogels (PA hydrogels)[30] and polyion-complex hydrogels (PIC hydrogels).[31] This two-stage recovery process is related to the competition between the elasticity of the primary chain and the strength of temporarily reformed physical bonds during the unloading process.

Hydrogels after UV Irradiation as a Rigid Component (First Network). To make the physical crosslinked hydrogel tough further by the introduction of chemical crosslinkers, the P(UM-*co*-NBOC) gels were irradiated with UV. As a typical example, we show the results of a P(UM-*co*-NBOC)-0.15 sample of 0.99 mm-thick. Upon UV irradiation, the gel became brownish, which is the color of 2-nitrobenzaldehyde, as a by-product (Figure 3a). The brownish color of samples became

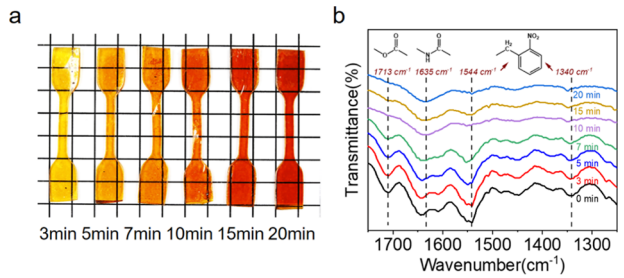

Figure 3. Photography (a) and the ATR/FT-IR absorption spectra (b) of UV irradiated P(UM-*co*-NBOC)-0.15 hydrogels with varied UV exposure times from both surfaces. After UV irradiation, the outer surface layers convert into P(UM-*co*-AMA) hydrogels. Initial sample thickness was 0.99 mm.

deeper with the increase of UV duration. These results suggest the cleavage of nitrobenzyl groups from NBOC moieties and the formation of 2-AMA. To get molecular evidence that the AMA attacks other ester bonds to form chemical crosslinking, the UV irradiated P(UM-*co*-NBOC) hydrogels with varied UV exposure times were characterized by attenuated total reflection Fourier-transform infrared spectroscopy (ATR/FT-IR) on an FT-IR 6600 spectrometer (JASCO, Japan) (Figure 3b). The absorbance peaks characteristic to nitro moieties (1340 and 1544 cm^{-1}) disappeared with the increase of UV exposure time, revealing the photocleavage of *o*-nitrobenzyl groups. Furthermore, the absorbance peak of ester carbonyl moieties (~1713 cm^{-1}) also considerably decreased with the exposure time, accompanied by the increase of the characteristic amide carbonyl absorbance peak at ~1635 cm^{-1}. These results clearly indicate the formation of amide linkages via either intrachain or interchain pathways. The latter contributes to effective chemical crosslinking.[26] Therefore, UV irradiation converts the pristine P(UM-*co*-NBOC) physical hydrogel into

DOI: 10.1021/acsami.9b13746
ACS Appl. Mater. Interfaces 2019, 11, 37139−37146

the P(UM-*co*-AMA) hydrogel that has both physical and chemical crosslinkings.

Gradient color changes along the depth direction of the sample are observed by photomicroscopy (Figure 4a).

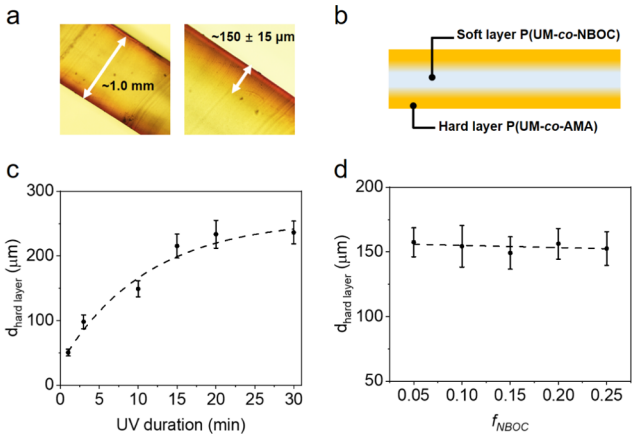

Figure 4. Composite structure formation of P(UM-*co*-NBOC) hydrogels by UV irradiation. (a) Cross-section micrographs with different magnifications of P(UM-*co*-NBOC)-0.15 hydrogels after UV irradiation from both sides. The thin bright layer near the surface is due to the optical effect. (b) Illustration of the sandwich structure formed by UV irradiation. (c) Dependence of hard outer layer thickness of P(UM-*co*-AMA)-0.15 hydrogels on UV irradiation duration. The initial sample thickness was 0.99 mm. (d) Hard outer layer thickness of P(UM-*co*-AMA) hydrogels with different f_{NBOC} after 10 min UV irradiation. The initial sample thickness was 0.99 mm. Each data was the average of 3−5 specimens of the same composition samples. Error bars represent standard deviation.

Therefore, after UV irradiation, only the surface layer of P(UM-*co*-NBOC) physical hydrogels was converted into the P(UM-*co*-AMA) hydrogels. Specifically, after 10 min of UV irradiation on both sides of the sample of 0.99 mm-thick, the gradient layer is ~150 μm thick (Figure 4a). The outmost surface layer of ~85 μm thick shows dense color, indicating the high photo-reaction and therefore higher chemical crosslinking density in this surface layer. The newly formed surface layers are stiffer than the inner layer. Accordingly, as illustrated in Figure 4b, a sandwich structure with two stiff outer layers of P(UM-*co*-AMA) and a soft middle layer of P(UM-*co*-NBOC) is formed. Thus, hydrogel composites composed of layers with different modulus could be easily generated.

The thickness of the UV curing is controlled by the UV penetration length. The factors influencing the depth of UV irradiation were studied. At a constant UV intensity, the depth of UV irradiation increased with the exposure time, and a saturated depth of 250 μm was reached after 30 min irradiation (Figure 4c). It should be noted that the exposure of the hydrogels under strong UV light longer than 10 min led to a temperature increase of the sample to a very high value (>60 °C), which may generate massive adverse reactions. Therefore, for the following samples, we only expose the hydrogels under UV light for 10 min. For P(UM-*co*-NBOC) hydrogels with different f_{NBOC}, the depth after 10 min UV irradiation kept around 150 μm, for all f_{NBOC} (Figure 4d).

To investigate the behavior of the P(UM-*co*-AMA) outer layer independently, thin P(UM-*co*-NBOC)-0.15 hydrogels of 0.29 mm-thick were fabricated. UV irradiation (10 min) of this sample gave a homogeneous stiff P(UM-*co*-AMA) hydrogel, taking into account the depth of color change upon UV irradiation (Figure 4a). The sample after UV irradiation was immersed in pure water to reach equilibrium. The gel showed the same brownish color, indicating that the hydrophobic by-product was trapped in the hydrogel. There was only a slight increase in the water-equilibrated volume (0.259 ± 0.011 vs 0.271 ± 0.010) of the hydrogel after UV irradiation, as well as the water content (20.04 ± 1.34 vs 21.02 ± 1.00 wt %), suggesting that the physical crosslinking of hydrophobic interactions is replaced by the newly formed chemical crosslink, but the disassembled physical crosslinkers are a little more than the newly formed chemical crosslinkers. Tensile tests were conducted to measure the mechanical properties of the P(UM-*co*-AMA) hydrogel (Figure 5a). Compared with the P(UM-*co*-NBOC)-0.15 hydrogel before UV irradiation, P(UM-*co*-AMA) gel has a higher Young's modulus but lower failure strain and stress (Figure 5b).

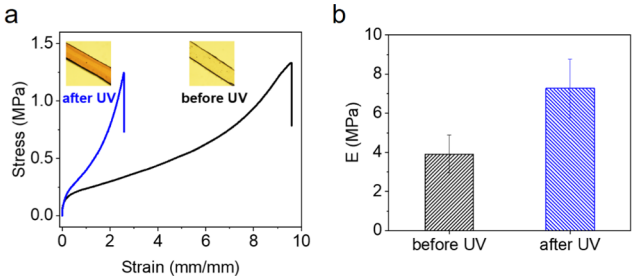

Figure 5. Effect of UV irradiation on the mechanical properties of P(UM-*co*-NBOC)-0.15. (a) Tensile stress−strain curves of the sample before and after UV irradiation. The inset images are cross-sectional micrographs of the sample. (b) Young's modulus (E) of hydrogels before and after UV irradiation from both sides. The sample thickness was 0.29 mm. The UV irradiation time was 10 min. Each data was the average of 3−5 specimens of the same composition samples. Error bars represent standard deviation.

Fabrication of DN Composite Hydrogel. The soft and highly stretchable hydrogel before UV and rigid and less stretchable after UV perfectly meet the requirements as soft and hard components, respectively, to construct composites with the feature of DN gel.[6,7]

The UV irradiated samples with a sandwich structure can be treated as layered composites. As the gels before and after UV irradiation did not significantly change the volume at swelling equilibrium states, the surface layer UV-cured samples had negligible stress mismatching at the interface and kept the flat shape.

To investigate the mechanical properties of the composite hydrogels, a series of P(UM-*co*-NBOC)-0.15 hydrogels with different thickness were irradiated with UV for 10 min. As the UV curing thickness was kept constant (~150 μm), the thickness ratio of hard outer layers to the soft middle layer was tuned by changing the overall sample thickness (Figure 6a). The tensile behaviors of samples with different thickness ratios are shown in Figure 6b. The one-component gels, of soft layer only (0/100) or hard layer only (100/0), showed a single yielding point, while a very remarkable second yielding point was observed for all of the sandwich gels at a strain of 1.6−1.8. With the increase of the thickness ratio of hard outer layers to the soft middle layer, the stress at the second yielding point increased, while the fracture strain decreased, which could be also obviously witnessed in Figure S1 for the fracture force.

DOI: 10.1021/acsami.9b13746
ACS Appl. Mater. Interfaces 2019, 11, 37139−37146

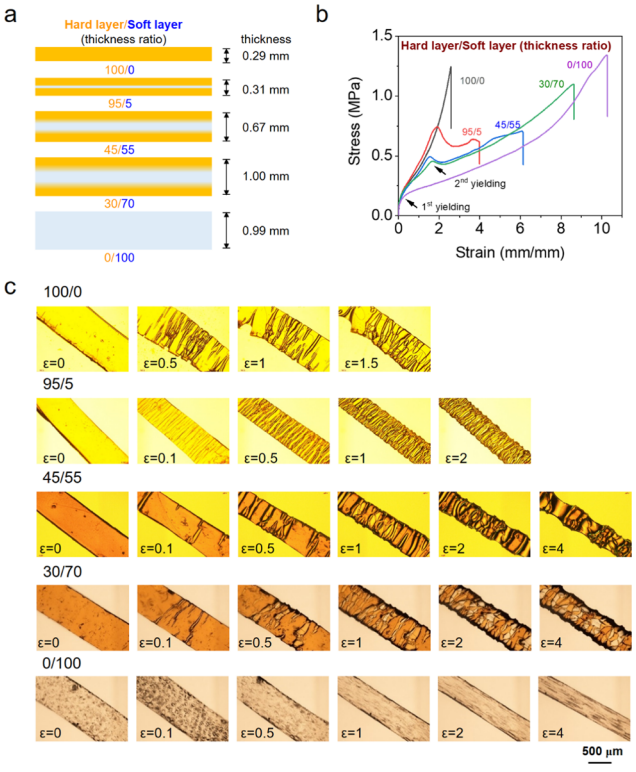

Figure 6. Composite hydrogels with a sandwiched layer structure composed of hard outer layers of the P(UM-*co*-AMA) hydrogel and the soft middle P(UM-*co*-NBOC) hydrogel. (a) Structure scheme, (b) tensile stress–strain curves with a different layer thickness ratio. The ratio was varied by UV irradiation to P(UM-*co*-NBOC)-0.15 hydrogels of different thickness from both sides of the sample. Each outer layer thickness was kept constant at 150 μm, while the middle layer thickness changes. (c) Optical microscope images of the sandwich hydrogel under stretching at different strains. The small drops on the surface of the pristine P(UM-*co*-NBOC) gel (0/100) at strain 0.1 were water drops placed on the gel surface to prevent drying.

The composite hydrogels follow the stress and strain curves of the pure hard sample (100/0) at small strains and then deviated to show lower stresses at large strains. It is interesting to see that the strain for the second yielding point was lower than the fracture strain of the homogeneous rigid sample (100/0), and decreased with the increase of the soft middle layer thickness. This result suggests that the soft middle layer makes the rigid outer layers break at a smaller strain in comparison with the free-standing rigid layer. The final fracture strain of the composites decreased with the increase of the hard/soft thickness ratio. The thinner the soft middle layer, the weaker the ability to bear the stretching and maintain global integrity. This is similar to the effect of the second network in DN gels. It has been shown that if the concentration of the second network is not high enough, then the gel would not be toughened effectively.

To reveal the fracture process, we further use optical microscopy to observe the structure change during the tensile process of the sandwich hydrogel (Figure 6c, Movie S1). The pristine soft hydrogel (0/100) before UV curing deformed homogeneously without crack formation before sample failure, while the rigid sample (100/0) showed craze above the first necking, and with the increase of strain, the craze density increased. The sandwich sample (95/5) showed well-defined dense crazes perpendicular to the elongation direction even at the very beginning of elongation (strain 0.1), corresponding to the first yielding point. The craze developed into branches with the increase of strain. With the increase of the thickness of the soft layer, both crazes perpendicular to the elongation direction and random irregular craze coexisted on the surface of the sandwich sample (45/55). The increased soft layer maintained the integrity of the whole sample; thus, the sample would not quickly break after the perpendicular craze grew into branches. On the other hand, the sandwich sample (30/70) showed irregular craze even at small strains (0.1), and at strain 2, above the second yielding point in the tensile curve, the hard outer layer broke into small fragments, and the soft middle layer became visible. With the further increase of strain, strong strain localization in the soft middle layer was observed. This result clearly shows that the hard layers, sustaining most of the load, broke first, while the soft middle layer maintained the integrity. The irregular craze in the sample (30/70) means that the cracks generated in the hard and less stretchable outer layers did not propagate since the middle layer, with increased strength, effectively carries the load.

It should be mentioned that even for the rigid 100/0 sample of 0.29 mm-thick, it showed surface craze before breaking (Figure 6c). This is due to the gradient chemical crosslinking within the rigid layer. As shown in Figure S2, when the sample thickness varies from 0.14 mm (=70 μm × 2) to 0.29 mm (= 145 μm × 2), the sample softened, accompanying with an increase in the fracture strain and decrease in fracture stress. Furthermore, more surface crack appeared before sample failure for the thick sample. These results indicate the effect of gradient structure on the behavior of the 100/0 sample of 0.29 mm-thick.

The yielding phenomenon has some common features with the yielding phenomenon in double-network (DN) gels. For DN gels, there is no strain localization before the yielding point. After the yielding point, part of the sample constricts as the necking zone, which subsequently grows with an increase in strain, and finally develops to the whole sample.[3] For our sandwich hydrogels, the appearance of the first percolated crack is reflected as the first yielding point and the crazing or fragmentation of the hard layers in the stress–strain curve, and the elongation of the middle layer between the cracks of the outer layers resemble the elongation of the second network in the necking zones of DN gels. In DN gels, usually, only one necking zone is generated and then it grows, while in the sandwich hydrogels, the crazes are generated over the whole sample surfaces. Such differences correspond to the yielding point and broad yielding peak in stress–strain curves for DN gels and sandwich hydrogels, respectively. This study shows that when the soft layer is relatively thin and weak, strip cracks are formed in the hard layers after yielding and the crack branches to break the layer into irregular fragmentation at enhanced strain. When the soft layer is relatively thick and strong, the crack grows irregularly to form irregular fragmentation right after yielding. The direct observation of the fracture process of the hard layers suggests that the internal fracture morphology of the first network in DN hydrogels would depend on the second network concentration.

The energy dissipation of the hydrogel composite is multi-scale. Breaking of the hard layers into small fragments and breaking of dynamic bonds of hydrophobic interactions in the soft middle layer both dissipated energies. The former is irreversible while the latter is reversible. Cyclic loading–

DOI: 10.1021/acsami.9b13746
ACS Appl. Mater. Interfaces 2019, 11, 37139–37146

unloading tests were conducted to evaluate the reversibility of energy dissipation U_{hys} of the sandwich hydrogel (30/70) (Figure 7). The sandwich hydrogel showed much larger

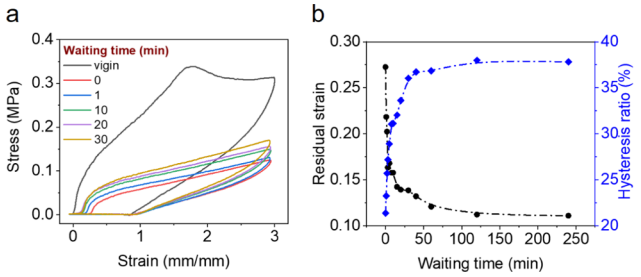

Figure 7. Self-recovery behaviors of the sandwich hydrogel (30/70). (a) Cyclic loading−unloading curves, and (b) residual strain and the hysteresis recovery ratio between the second and first loading cycles for different waiting times.

hysteresis (Figure 7a) than its original P(UM-*co*-NBOC) gel in the first loading−unloading cycle (Figure 2a). It indicates more dissipation of energy contributed by the newly formed chemical crosslinkers instead of physical crosslinkers and the extensibility came from the soft inner layer, P(UM-*co*-NBOC). The hysteresis area U_{hys} enclosed by the first loading−unloading cycle is up to 64% of the work of extension W, while that for hydrogel before UV irradiation is 56%. However, the sandwich hydrogel cannot fully recover due to its chemical crosslinked network origin (Figure 7b). The residual strain and hysteresis showed dependence with waiting time, and the recovery also included two stages. However, the hysteresis recovery ratio reached only 38% of the hysteresis area in the first loading−unloading cycle (Figure 6b). This is related to the breaking of unrecoverable chemical bonds after UV irradiation.

Since UV light can be easily controlled, we further use UV mask to fabricate the pattern hydrogels with different modulus regions. For instance, a two-dimensional (2D)-patterned hydrogel, composed of alternating P(UM-*co*-NBOC) and P(UM-*co*-AMA) structures, was prepared from the thin P(UM-*co*-NBOC) hydrogel, to which UV light could penetrate the whole sample (Figure S3). It showed similar Young's modulus and fracture strain compared with the pure P(UM-*co*-AMA) samples, while there was a yielding near the fracture strain, because of the fracture of the UV irradiated domains and the deformation of no irradiation domains. When we irradiate a thick P(UM-*co*-NBOC) gel with a UV mask, a three-dimensional (3D)-patterned hydrogel can be fabricated, which has a structure of two outer layers of 2D-patterned gels with a homogeneous middle layer of P(UM-*co*-NBOC). The tensile stress−strain curve of the 3D-patterned hydrogel is very similar to that of sandwich-like hydrogels (Figure S3).

CONCLUSIONS

Based on the addition of hydrophobic interaction by copolymerization of UM with NBOC, the mechanical properties, toughness, and fatigue resistance of P(UM-*co*-NBOC) hydrogels improved dramatically. Upon UV irradiation, part of physical crosslinkers composed of hydrophobic interaction transformed into chemical crosslinkers, which further enhance the mechanical properties. By controlling the UV irradiation depth and position, the hybrid hydrogel consisting of different modulus regions can be easily prepared. This work provides a new strategy to fabricate tough hydrogel composites by incorporating a photoresponsive hydrophobic residue into the hydrogel network. Besides, it could be taken as a simple macroscopic model for further understanding of the DN toughening mechanism.

ASSOCIATED CONTENT

Supporting Information

The Supporting Information is available free of charge on the ACS Publications website at DOI: 10.1021/acsami.9b13746.

Tensile force−strain curves of the composite hydrogels with the sandwiched layer structure of different layer thickness ratios; results of mechanical tests for one-component hydrogel composed of only a hard layer with varied thickness; scheme and results of mechanical tests of the patterned composite hydrogel (PDF)

Tensile process of the composite hydrogel (Movie S1) (MP4)

AUTHOR INFORMATION

Corresponding Author

*E-mail: gong@sci.hokudai.ac.jp.

ORCID

Jian Ping Gong: 0000-0003-2228-2750

Notes

The authors declare no competing financial interest.

ACKNOWLEDGMENTS

This research was supported by JSPS KAKENHI Grant Numbers JP17H06144. The Institute for Chemical Reaction Design and Discovery (ICReDD) was established by the World Premier International Research Initiative (WPI), MEXT, Japan.

REFERENCES

(1) Gong, J. P.; Katsuyama, Y.; Kurokawa, T.; Osada, Y. Double-Network Hydrogels with Extremely High Mechanical Strength. *Adv. Mater.* **2003**, *15*, 1155−1158.

(2) Gong, J. P. Why Are Double Network Hydrogels So Tough? *Soft Matter* **2010**, *6*, 2583−2590.

(3) Nakajima, T.; Kurokawa, T.; Ahmed, S.; Wu, W.-l.; Gong, J. P. Characterization of Internal Fracture Process of Double Network Hydrogels under Uniaxial Elongation. *Soft Matter* **2013**, *9*, 1955−1966.

(4) Matsuda, T.; Nakajima, T.; Fukuda, Y.; Hong, W.; Sakai, T.; Kurokawa, T.; Chung, U.-i.; Gong, J. P. Yielding Criteria of Double Network Hydrogels. *Macromolecules* **2016**, *49*, 1865−1872.

(5) Wang, X.; Hong, W. Pseudo-Elasticity of A Double Network Gel. *Soft Matter* **2011**, *7*, 8576−8581.

(6) Feng, X.; Ma, Z.; MacArthur, J. V.; Giuffre, C. J.; Bastawros, A. F.; Hong, W. A Highly Stretchable Double-Network Composite. *Soft Matter* **2016**, *12*, 8999−9006.

(7) Takahashi, R.; Sun, T. L.; Saruwatari, Y.; Kurokawa, T.; King, D. R.; Gong, J. P. Creating Stiff, Tough, and Functional Hydrogel Composites with Low-Melting-Point Alloys. *Adv. Mater.* **2018**, *30*, No. e1706885.

(8) Cooper, C. B.; Joshipura, I. D.; Parekh, D. P.; Norkett, J.; Mailen, R.; Miller, V. M.; Genzer, J.; Dickey, M. D. Toughening Stretchable Fibers via Serial Fracturing of A Metallic Core. *Sci. Adv.* **2019**, *5*, No. eaat4600.

(9) Hong, S.; Sycks, D.; Chan, H. F.; Lin, S.; Lopez, G. P.; Guilak, F.; Leong, K. W.; Zhao, X. 3D Printing of Highly Stretchable and Tough Hydrogels into Complex, Cellularized Structures. *Adv. Mater.* **2015**, *27*, 4035−4040.

DOI: 10.1021/acsami.9b13746
ACS Appl. Mater. Interfaces 2019, 11, 37139−37146

(10) Fan, H.; Wang, J.; Jin, Z. Tough, Swelling-Resistant, Self-Healing, and Adhesive Dual-Cross-Linked Hydrogels Based on Polymer−Tannic Acid Multiple Hydrogen Bonds. *Macromolecules* **2018**, *51*, 1696−1705.
(11) Lin, P.; Ma, S.; Wang, X.; Zhou, F. Molecularly Engineered Dual-Crosslinked Hydrogel with Ultrahigh Mechanical Strength, Toughness, and Good Self-Recovery. *Adv. Mater.* **2015**, *27*, 2054−2059.
(12) Huang, Y.; King, D. R.; Sun, T. L.; Nonoyama, T.; Kurokawa, T.; Nakajima, T.; Gong, J. P. Energy-Dissipative Matrices Enable Synergistic Toughening in Fiber Reinforced Soft Composites. *Adv. Funct. Mater.* **2017**, *27*, No. 1605350.
(13) Gojny, F. H.; Wichmann, M. H. G.; Fiedler, B.; Bauhofer, W.; Schulte, K. Influence of Nano-Modification on The Mechanical and Electrical Properties of Conventional Fibre-Reinforced Composites. *Composites, Part A* **2005**, *36*, 1525−1535.
(14) Cheng, Q.; Li, M.; Jiang, L.; Tang, Z. Bioinspired Layered Composites Based on Flattened Double-Walled Carbon Nanotubes. *Adv. Mater.* **2012**, *24*, 1838−1843.
(15) Huang, T.; Xu, H. G.; Jiao, K. X.; Zhu, L. P.; Brown, H. R.; Wang, H. L. A Novel Hydrogel with High Mechanical Strength: A Macromolecular Microsphere Composite Hydrogel. *Adv. Mater.* **2007**, *19*, 1622−1626.
(16) Sudre, G.; Olanier, L.; Tran, Y.; Hourdet, D.; Creton, C. Reversible Adhesion Between A Hydrogel and A Polymer Brush. *Soft Matter* **2012**, *8*, 8184−8193.
(17) Keplinger, C.; Sun, J. Y.; Foo, C. C.; Rothemund, P.; Whitesides, G. M.; Suo, Z. Stretchable, Transparent, Ionic Conductors. *Science* **2013**, *341*, 984−987.
(18) Sun, J. Y.; Keplinger, C.; Whitesides, G. M.; Suo, Z. Ionic Skin. *Adv. Mater.* **2014**, *26*, 7608−7614.
(19) Yang, C. H.; Chen, B. H.; Lu, J. J.; Yang, J. H.; Zhou, J. X.; Chen, Y. M.; Suo, Z. G. Ionic Cable. *Extreme Mech. Lett.* **2015**, *3*, 59−65.
(20) Han, L.; Lu, X.; Liu, K.; Wang, K.; Fang, L.; Weng, L. T.; Zhang, H.; Tang, Y.; Ren, F.; Zhao, C.; Sun, G.; Liang, R.; Li, Z. Mussel-Inspired Adhesive and Tough Hydrogel Based on Nanoclay Confined Dopamine Polymerization. *ACS Nano* **2017**, *11*, 2561−2574.
(21) Yuk, H.; Zhang, T.; Parada, G. A.; Liu, X.; Zhao, X. Skin-Inspired Hydrogel-Elastomer Hybrids with Robust Interfaces and Functional Microstructures. *Nat. Commun.* **2016**, *7*, No. 12028.
(22) Yuk, H.; Zhang, T.; Lin, S.; Parada, G. A.; Zhao, X. Tough Bonding of Hydrogels to Diverse Non-Porous Surfaces. *Nat. Mater.* **2016**, *15*, 190−196.
(23) Zhang, X.; Pint, C. L.; Lee, M. H.; Schubert, B. E.; Jamshidi, A.; Takei, K.; Ko, H.; Gillies, A.; Bardhan, R.; Urban, J. J.; Wu, M.; Fearing, R.; Javey, A. Optically- and Thermally-Responsive Programmable Materials Based on Carbon Nanotube-Hydrogel Polymer Composites. *Nano Lett.* **2011**, *11*, 3239−3244.
(24) Kim, M.; Jung, B.; Park, J. H. Hydrogel Swelling as A Trigger to Release Biodegradable Polymer Microneedles in Skin. *Biomaterials* **2012**, *33*, 668−678.
(25) Tanaka, T.; Sun, S. T.; Hirokawa, Y.; Katayama, S.; Kucera, J.; Hirose, Y.; Amiya, T. Mechanical Instability of Gels at the Phase-Transition. *Nature* **1987**, *325*, 796−798.
(26) Wang, X.; Liu, G.; Hu, J.; Zhang, G.; Liu, S. Concurrent Block Copolymer Polymersome Stabilization and Bilayer Permeabilization by Stimuli-Regulated. *Angew. Chem., Int. Ed.* **2014**, *53*, 3138−3142.
(27) Nakajima, T.; Furukawa, H.; Tanaka, Y.; Kurokawa, T.; Osada, Y.; Gong, J. P. True Chemical Structure of Double Network Hydrogels. *Macromolecules* **2009**, *42*, 2184−2189.
(28) Yang, Y.; Wang, X.; Yang, F.; Shen, H.; Wu, D. A Universal Soaking Strategy to Convert Composite Hydrogels into Extremely Tough and Rapidly Recoverable Double-Network Hydrogels. *Adv. Mater.* **2016**, *28*, 7178−7184.
(29) Fukao, K.; Nonoyama, T.; Kiyama, R.; Furusawa, K.; Kurokawa, T.; Nakajima, T.; Gong, J. P. Anisotropic Growth of Hydroxyapatite in Stretched Double Network Hydrogel. *ACS Nano* **2017**, *11*, 12103−12110.
(30) Sun, T. L.; Kurokawa, T.; Kuroda, S.; Ihsan, A. B.; Akasaki, T.; Sato, K.; Haque, M. A.; Nakajima, T.; Gong, J. P. Physical Hydrogels Composed of Polyampholytes Demonstrate High Toughness and Viscoelasticity. *Nat. Mater.* **2013**, *12*, 932−937.
(31) Luo, F.; Sun, T. L.; Nakajima, T.; Kurokawa, T.; Zhao, Y.; Sato, K.; Ihsan, A. B.; Li, X.; Guo, H.; Gong, J. P. Oppositely Charged Polyelectrolytes form Tough, Self-Healing, and Rebuildable Hydrogels. *Adv. Mater.* **2015**, *27*, 2722−2727.

DOI: 10.1021/acsami.9b13746
ACS Appl. Mater. Interfaces 2019, 11, 37139−37146